# Structural Analyses of Nucleotide Binding to an Aminoglycoside Phosphotransferase[†,‡]

D. L. Burk, W. C. Hon,[§] A. K.-W. Leung,[||] and A. M. Berghuis*

*Antimicrobial Research Centre and Department of Biochemistry, McMaster University, Hamilton, Ontario, Canada L8N 3Z5*

*Received March 12, 2001; Revised Manuscript Received May 11, 2001*

ABSTRACT: 3′,5″-Aminoglycoside phosphotransferase type IIIa [APH(3′)-IIIa] is a bacterial enzyme that confers resistance to a range of aminoglycoside antibiotics while exhibiting striking homology to eukaryotic protein kinases (ePK). The structures of APH(3′)-IIIa in its apoenzyme form and in complex with the nonhydrolyzable ATP analogue AMPPNP were determined to 3.2 and 2.4 Å resolution, respectively. Furthermore, refinement of the previously determined ADP complex was completed. The structure of the apoenzyme revealed alternate positioning of a flexible loop (analogous to the P-loop of ePK's), occupying part of the nucleotide-binding pocket of the enzyme. Despite structural similarity to protein kinases, there was no evidence of domain movement associated with nucleotide binding. This rigidity is due to the presence of more extensive interlobe interactions in the APH(3′)-IIIa structure than in the ePK's. Differences between the ADP and AMPPNP complexes are confined to the area of the nucleotide-binding pocket. The position of conserved active site residues and magnesium ions remains unchanged, but there are differences in metal coordination between the two nucleotide complexes. Comparison of the di/triphosphate binding site of APH(3′)-IIIa with that of ePK's suggests that the reaction mechanism of APH(3")-IIIa and related aminoglycoside kinases will closely resemble that of eukaryotic protein kinases. However, the orientation of the adenine ring in the binding pocket differs between APH(3′)-IIIa and the ePK's by a rotation of approximately 40°. This alternate binding mode is likely a conserved feature among aminoglycoside kinases and could be exploited for the structure-based drug design of compounds to combat antibiotic resistance.

The discovery of antimicrobial compounds such as penicillin in the early 20th century ushered in the era of antibiotics as "wonder drugs". These compounds have proven to be of great value in medicine and have revolutionized the treatment of infectious disease. However, the increased use of antibiotics in the last half of the 20th century, both in medicine and in the food industry, has been accompanied by a concomitant increase in bacterial resistance to these compounds. Clinically important resistance to an antibiotic may appear within months of its introduction (*1*), and multidrug resistance is now the major cause of failure in the treatment of infectious disease (*2*).

The aminoglycosides are a class of broad-spectrum antimicrobial compounds, including streptomycin, kanamycin, and gentamicin, with potent and rapid bactericidal properties (*3*). They are used, for example, in conjunction with penicillin, ampicillin, and vancomycin to treat serious enterococcal infections, endocarditis, urinary tract, and intraabdominal infections (*4*). Aminoglycosides exert their antimicrobial effects by binding to the 30S subunit of the bacterial ribosome and obstructing protein synthesis (*5*). This leads to a loss of bacterial cell wall integrity via a mechanism that remains unclear (*6*). Although resistance to aminoglycoside antibiotics as a result of alterations to their ribosomal binding site or as a consequence of a change in the permeability of the cell has been implicated, the major mechanism of bacterial resistance to aminoglycosides is the chemical modification by bacterial enzymes (*3*). These aminoglycoside-modifying enzymes are a large and diverse group that fall into three general classes, depending on the identity of the chemical group used to modify the antibiotic. These classes are aminoglycoside *O*-phosphotransferases (APH's),[1] aminoglycoside *O*-adenyltransferases (ANT's), and aminoglycoside *N*-acetyltransferases (AAC's). Enzymatic modification of aminoglycoside antibiotics via APH's,

[†] This work was funded by a grant from the Canadian Institutes for Health Research to A.M.B. (MT-13107). A.M.B. is the recipient of a CIHR/PMAC-HRF Research Career Award.

[‡] The atomic coordinates of 3′,5″-aminoglycoside phosphotransferase [APH(3′)-IIIa] and its complexes with ADP and AMPPNP have been deposited with the Protein Data Bank (accession numbers 1J7I, 1J7L, and 1J7U).

* To whom correspondence should be addressed. E-mail: berghuis@mcmaster.ca. Telephone: (905) 525-9140 ext 22316. Fax: (905) 522-9033.

[§] Present address: Division of Structural Biology, Wellcome Trust Centre for Human Genetics, University of Oxford, Oxford, U.K. OX3 7BN.

[||] Present address: Structural Studies Division, MRC Laboratory of Molecular Biology, Hills Road, Cambridge, U.K. CB2 2QH.

[1] Abbreviations: AAC, aminoglycoside *N*-acetyltransferase; ADP, adenosine 5′-diphosphate; AMPPNP, adenosine 5′-($\beta$,$\gamma$-imino)triphosphate; ANT, aminoglycoside *O*-adenyltransferase; APH, aminoglycoside *O*-phosphotransferase; APH(3′), 3′-aminoglycoside phosphotransferase; APH(3′)-IIIa, 3′,5″-aminoglycoside phosphotransferase type IIIa; ATP, adenosine 5′-triphosphate; cAPK, cyclic AMP dependent protein kinase; EDTA, ethylenediaminetetraacetic acid; ePK, eukaryotic protein kinase; HEPES, *N*-(2-hydroxyethyl)piperazine-*N*′-2-ethanesulfonic acid; NCS, noncrystallographic symmetry; Phk$\gamma$, glycogen phosphorylase kinase $\gamma$ subunit; rmsd, root mean squared deviation.

10.1021/bi010504p CCC: $20.00 
Published on Web 07/06/2001

ANT's, and AAC's has been found in most clinically relevant Gram-positive and Gram-negative bacteria (*7*).

There are a number of types of aminoglycoside phosphotransferases (APH's), each with a characteristic substrate profile (*3*). The largest class, APH(3′), catalyzes the modification of 4,5- and 4,6-disubstituted aminoglycosides at the 3′-hydroxyl position. One member of this class, APH(3′)-IIIa, is found in Gram-positive cocci such as Staphylococci and Enterococci. This enzyme has the broadest substrate specificity of the APH(3′) isozymes, phosphorylating at least nine different aminoglycoside substrates and carrying out additional phosphorylation of 4,5-disubstituted antibiotics at the 5″ positions (*8*, *9*). The enzyme catalyzes this reaction via a Theorell−Chance mechanism in which the enzyme first binds ATP and $Mg^{2+}$ ions, followed by aminoglycoside. After transferring the $\gamma$-phosphate from ATP, the enzyme releases the phosphorylated aminoglycoside, followed by ADP. The slow release of ADP has been shown to be the rate-limiting step in the overall reaction (*10*). Although the details of the mechanism by which the enzyme carries out phosphoryl transfer remain unclear, there is evidence from mutagenesis studies, solvent isotope, and solvent viscosity experiments that indicates direct transfer of the phosphate group and a dissociative-like transition state (*11*−*13*).

APH(3′)-IIIa is the only aminoglycoside phosphotransferase to have its three-dimensional atomic structure characterized. The structure was solved to 2.2 Å resolution by X-ray crystallography in complex with ADP (*12*). The enzyme is bilobal, with an N-terminal lobe consisting mainly of a five-stranded antiparallel $\beta$-sheet and a largely α-helical C-terminal lobe. The nucleotide-binding site lies in a cleft between the two lobes. Surprisingly, the structure revealed significant structural similarity between APH(3′)-IIIa and ePK's. Despite low amino acid sequence homology of <5%, over 40% of the APH(3′)-IIIa molecule is structurally similar to ePK's such as cAMP-dependent protein kinase (cAPK) (*12*). It has subsequently been shown that APH(3′)-IIIa is also functionally similar to eukaryotic protein kinases in that it phosphorylates a range of peptide and protein substrates (*14*). Furthermore, several protein kinase inhibitors have been shown to also inhibit APH(3′)-IIIa activity (*15*).

Our ultimate goal is to understand the reaction mechanism of the APH(3′)-IIIa enzyme at the atomic level. Toward this end, we have solved the three-dimensional atomic structures of two additional intermediates in the APH(3′)-IIIa reaction cycle—the APH(3′)-IIIa in complex with the nonhydrolyzable ATP analogue AMPPNP and the APH(3′)-IIIa apoenzyme (i.e., with no nucleotide cofactor). These structures will help to advance our understanding of the mechanism by which APH(3′)-IIIa inactivates aminoglycosides.

## EXPERIMENTAL PROCEDURES

*Protein Purification and Crystallization.* Recombinant APH(3′)-IIIa was expressed and purified by differential ammonium sulfate precipitation and anion-exchange chromatography as described previously (*8*). Crystals of the APH(3′)-IIIa·AMPPNP binary complex were grown by the hanging drop vapor diffusion method, using PEG 4000 and 2-propanol as crystallizing agents. Drops containing 2−3 $\mu$L of a protein−AMPPNP solution [8 mg/mL protein; 1 mM AMPPNP (Mg salt); 5 mM HEPES, pH 7.5; 10 mM $MgCl_2$] were combined with 2−3 $\mu$L of a well solution consisting of 100 mM HEPES, pH 7.5, 20% PEG 4000 (w/v), and 10% 2-propanol (v/v). The drops were placed on siliconized cover slips and suspended over wells containing 500 $\mu$L of the well solution and stored at room temperature. Diffraction quality crystals (with approximate dimensions 0.4 × 0.1 × 0.05 mm) were observed within 1 week.

Table 1: Data Collection Statistics for the APH(3′)-IIIa Complexes

| | APH(3′)-IIIa·ADP[a] | APH(3′)-IIIa·AMPPMP | APH(3′)-IIIa (apo) |
|---|---|---|---|
| space group | $P2_12_12_1$ | $P2_12_12_1$ | $P4_32_12$ |
| cell dimensions | | | |
| *a* (Å) | 49.7 | 50.2 | 55.7 |
| *b* (Å) | 91.3 | 91.3 | 55.7 |
| *c* (Å) | 131.3 | 132.7 | 185.2 |
| resolution (Å)[b] | 2.2 (2.28−2.20) | 2.4 (2.49−2.40) | 3.2 (3.31−3.20) |
| total observations | 95428 | 92600 | 15937 |
| unique observations | 30902 | 24507 | 5165 |
| $R_{merge}$[b,c] | 0.055 (0.213) | 0.055 (0.197) | 0.139 (0.495) |
| $I/\sigma_I$[b] | 13.9 (4.7) | 19.5 (3.0) | 7.2 (2.3) |
| completeness[b] | 96.4 (95.9) | 99.2 (97.9) | 97.3 (96.7) |

[a] Data collection statistics for the APH(3′)-IIIa·ADP complex were published previously (*12*) and are provided here for comparison purposes. [b] Number in parentheses refers to highest resolution shell. [c] $R_{merge} = \sum|I_i - \langle I\rangle|/\sum I_i$, where $I$ represents the intensities of a multiply measured reflection *hkl* and $\langle I\rangle$ their average.

Crystals of the APH(3′)-IIIa apoenzyme were grown at room temperature by the hanging drop vapor diffusion method using ammonium sulfate and 2-propanol as precipitants. Hanging drops (4−6 $\mu$L), consisting of protein solution (8 mg/mL protein; 5 mM HEPES, pH 7.5; 10 mM $MgCl_2$) and an equal volume of well solution, were suspended from a siliconized cover slip over a well containing 500 $\mu$L of a 2 M ammonium sulfate (w/v) and 5% 2-propanol (v/v) solution. Diffraction quality crystals (with approximate dimensions of 0.4 × 0.3 × 0.1 mm) were observed in these drops within approximately 1 week.

*Data Collection and Processing.* X-ray diffraction data were collected from single crystals of the APH(3′)-IIIa·AMPPNP complex and the APH(3′)-IIIa apoenzyme on a Rigaku R-AXIS IIc area detector system. The detector was used with a Rigaku RU-200 rotating-anode X-ray generator (equipped with Supper double-focusing mirrors) operating at 50 kV and 60 mA. Data for the AMPPNP complex were obtained under cryogenic conditions (106 K). To protect the APH(3′)-IIIa·AMPPNP crystal during the freezing procedure, the crystal was briefly placed in mother liquor that had its PEG 4000 concentration increased from 20% to 30%. The crystal was then removed from the cryoprotectant and immediately frozen by immersing it in liquid nitrogen. The crystal was then placed on the goniometer head in the cooled nitrogen stream. Due to the sensitivity of the apoenzyme crystals to freezing, data collection with this crystal was done at room temperature.

The diffraction data collected from both the AMPPNP complex and apoenzyme were indexed, integrated, and scaled using the programs Denzo and Scalepack (*16*). Statistics associated with the data collection and processing are shown in Table 1.

*Structure Determination and Refinement.* The structure of the APH(3′)-IIIa·ADP complex was solved previously using

Table 2: Refinement Statistics for APH(3′)-IIIa Complexes

| | APH(3′)-IIIa·ADP[a] | APH(3′)-IIIa·AMPPMP[a] | APH(3′)-IIIa (apo) |
|---|---|---|---|
| resolution range (Å) | 50.0−2.2 | 50.0−2.4 | 50.0−3.2 |
| no. of reflections used ($F/\sigma_F > 0$) | 30902 | 23957 | 4829 |
| $R_{cryst}$[b] | 0.220 | 0.217 | 0.219 |
| $R_{free}$[c] | 0.279 | 0.277 | 0.306 |
| no. of protein atoms | 4344[§] | 4344[§] | 2148 |
| no. of cofactor atoms | 54 | 62 | 0 |
| no. of water molecules | 308 | 188 | 0 |
| no. of $Mg^{2+}$ ions | 4 | 4 | 0 |
| rmsd bonds (Å) | 0.006 | 0.008 | 0.007 |
| rmsd angles (deg) | 1.219 | 1.251 | 1.341 |
| coordinate error (Å)[d] | 0.21 | 0.19 | 0.19 |

[a] Two molecules in the asymmetric unit. [b] $R_{cryst} = \sum|F_o - F_c|/\sum F_o$. [c] $R_{free}$ is the crystallographic *R*-factor calculated from 10% of the data not included in refinement. [d] Estimate using cross-validated $\sigma_A$ plots.

MAD data from a Se-Met derivative (*12*). Before being used in the comparisons described here, the structure of this complex was subjected to additional refinement with the CNS program package (*17*). Each round of refinement consisted of 200 steps of conjugate gradient positional refinement, followed by 30 steps of restrained individual thermal factor refinement. Refinement of this model was carried out using all data between 50 and 2.2 Å and employed bulk solvent corrections and a maximum likelihood (using amplitudes) target function. After each round of refinement, $\sigma_A$-weighted $2F_o - F_c$ and $F_o - F_c$ difference electron density maps were calculated and inspected (*18*). During these inspections, manual adjustments were made to the model, and ordered solvent molecules were added at $F_o - F_c$ difference peaks if they could form reasonable hydrogen bond interactions with protein atoms and/or solvent molecules. Refinement continued in this fashion until the conventional and free *R*-values could no longer be improved (*19*, *20*). The result of the additional refinement was a reduction in the $R_{free}$ from 0.301 to 0.279 using all data (*21*−*23*). Final refinement statistics for this APH(3′)-IIIa·ADP model, as well as for the AMPPNP complex and the apoprotein, are given in Table 2.

The APH(3′)-IIIa·ADP structure was used as the starting model for the refinement of the APH(3′)-IIIa·AMPPNP complex. The ADP molecule was included in the model, but the active site magnesium ions were omitted, as were all solvent molecules within approximately 5 Å of the nucleotide and those with thermal factors greater than 30 Å$^2$. The refinement procedure followed was analogous to that described for the APH(3′)-IIIa·ADP complex. Rounds of positional and individual thermal factor refinement using all data between 50 and 2.4 Å were followed by examination of $\sigma_A$-weighted electron density maps. After the first round, clear peaks were observed in the $F_o - F_c$ difference electron density map into which the terminal phosphate groups of the two AMPPNP molecules (one per protein molecule) could be modeled. Electron density was also observed for the active site magnesium ions in both protein molecules, and these were added to the refinement model. There was some evidence for metal-coordinated solvent atoms, but these were not introduced at this time. Noncrystallographic symmetry (NCS) restraints between the two AMPPNP molecules and between the two pairs of active site $Mg^{2+}$ ions in the asymmetric unit were introduced at this stage to restrain their positions. During subsequent refinement rounds, convincing electron density for magnesium-coordinated water molecules became apparent. These were then added to the model and their positions restrained using NCS. Other ordered solvent molecules were also added at $F_o - F_c$ difference map peaks, if they formed reasonable hydrogen bonds to protein atoms and/or solvent molecules. When conventional and free *R*-values could no longer be improved, refinement was stopped.

The structure of the APH(3′)-IIIa apoenzyme was solved using molecular replacement techniques as implemented in the program X-PLOR (*24*). The search model consisted of the structure of the APH(3′)-IIIa·ADP complex, with ADP cofactor, magnesium ion, and water molecules removed. A rotation search using diffraction data between 10 and 4 Å and with $F/\sigma_F > 2.0$ yielded one solution that was significantly better than the others. Following PC refinement of the rotation solutions, a translation search was undertaken using the top rotation solution and data between 15 and 4 Å ($F/\sigma_F > 2.0$). The top solution from the translation search was then subjected to rigid-body refinement, followed by steps of positional and grouped thermal factor refinement in CNS using all data between 50 and 3.2 Å. Following each refinement round, $\sigma_A$-weighted $2F_o - F_c$ and $F_o - F_c$ difference electron density maps were calculated, and manual adjustments were made to the model as necessary. The most significant rebuilding of the model was required for residues 22−29, 100−112, and 147−170. Due to the moderate resolution of the apoenzyme diffraction data set, no attempt was made to model ordered solvent molecules. As with the other structures, rounds of refinement were continued until no further improvements in the conventional and free *R*-values were observed.

## RESULTS

*Model Stereochemistry.* The models of APH(3′)-IIIa in complex with ADP or AMPPNP and in the apoenzyme form exhibit satisfactory geometry, with no residues falling in the disallowed region of a Ramachandran plot calculated using the program PROCHECK (*25*, *26*). The ADP and AMPPNP complexes have 90.0% and 88.3% of their non-glycine, non-proline residues in the most favored region of the Ramachandran plot, respectively. The corresponding value for the apoenzyme structure is 80.7%. A small number of residues fall into generously allowed regions of the plot. These residues are located in loop regions of the protein with above-average thermal factors and ambiguous electron density.

*Peptide Backbone.* The ADP and AMPPNP complexes crystallized with two molecules in the asymmetric unit of space group $P2_12_12_1$. The two molecules in the asymmetric unit were superimposed using the coordinates of all main chain atoms and the least-squares method as implemented in the program LSQMAN (*27*). The overall rmsd for all main chain atoms between the two molecules in both the asymmetric units of the ADP and AMPPNP complexes is 0.6 Å. These numbers are somewhat misleading, however, since a large part of the positional variability between the two molecules in the asymmetric unit is localized to three areas (residues 100−112, 147−170, and 226−238).

Residues 100−112 constitute the end of helix α3, the first few residues of α4, and the intervening loop segment

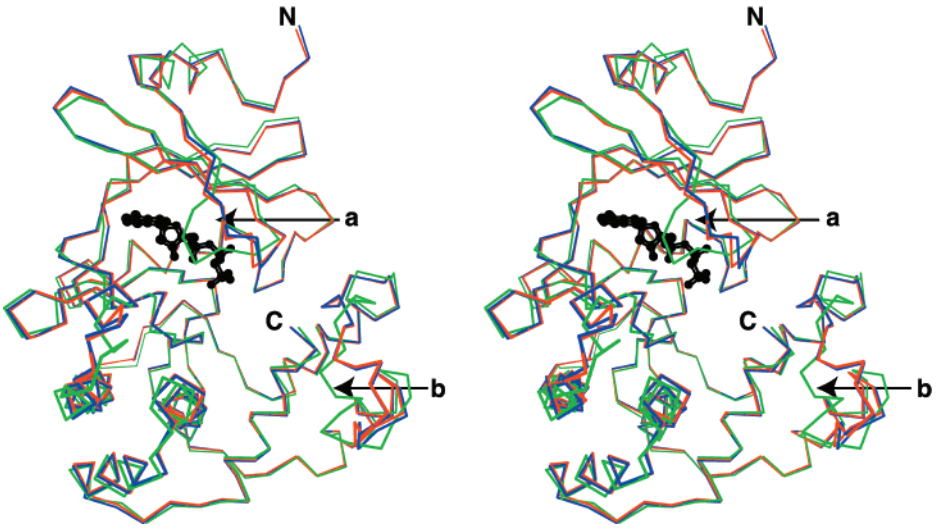


FIGURE 1: Stereoview of the α carbon trace of the APH(3′)-IIIa·ADP (red), APH(3′)-IIIa·AMPPNP (blue), and APH(3′)-IIIa apoenzyme (green) structures. The AMPPNP molecule is drawn in black to highlight the nucleotide-binding pocket. Two areas of significant positional deviation are highlighted: (a) the loop over the nucleotide-binding pocket (residues 22−29) and (b) the antibiotic-binding pocket (residues 147−170).

(secondary structural nomenclature follows that of ref *12*). This section of polypeptide includes the tethering segment joining the N- and C-terminal domains of the APH(3′)-IIIa structure. The electron density in these areas is of poor quality, and the residues in this region exhibit higher than average thermal factors.

The second region of above average positional deviation between the APH(3′)-IIIa structures is residues 147−170. This section of the protein includes the ends of helices αA and αB, and the intervening loop—a region proposed to form part of the aminoglycoside-binding site in APH(3′)-IIIa (*12*). This region possesses some sequence similarity in the APH(3′) isozymes but has no analogue in the structures of eukaryotic protein kinases. This extended loop structure forms a flap over the outside edge of the nucleotide-binding pocket, where it is believed to participate in the formation of a binding site for substrates. The differences observed between the two molecules in the asymmetric unit of the ADP and AMPPNP complexes are a result of differences in crystal packing for the APH(3′)-IIIa molecules, compounded by the presence of a intermolecular disulfide bond linking Cys156 to Cys19 of the second molecule in the asymmetric unit. However, under physiological conditions this disulfide bond is absent, and therefore the different conformations observed for residues 147−150 reflect the intrinsic, and probably functionally important, flexible nature of this segment of the protein structure.

Residues 226−238 include a loop region of the APH(3′)-IIIa molecule, as well as the terminal segments of helices α5 and αC. This loop region has higher than average thermal factors and poorly defined electron density. The observed positional differences are therefore again a consequence of inherent backbone flexibility in this section of the polypeptide chain.

If these three regions of the polypeptide chain (residues 100−112, 147−170, and 226−238) are excluded from the rmsd calculation, the values become 0.3 Å for both the molecules in the ADP and AMPPNP asymmetric units. These values are comparable to the estimated error of the coordinates (∼0.2 Å, Table 2). Due to the high degree of similarity between the two molecules in the asymmetric unit outside of these poorly defined regions, the coordinates of a single molecule from the asymmetric unit were used for subsequent comparison between the APH(3′)-IIIa·ADP, APH(3′)-IIIa·AMPPNP, and apoenzyme structures.

The structures of the APH(3′)-IIIa·ADP, APH(3′)-IIIa·AMPPNP, and APH(3′)-IIIa apoenzyme species were superimposed with LSQMAN as described above. The apoenzyme superimposes with both the ADP and the AMPPNP complexes with an rmsd of 1.5 Å. The value for the superposition of the two nucleotide-bound complexes is 0.3 Å. These results are depicted graphically in Figure 1, which shows the polypeptide backbones of the three structures following least-squares superposition (where a and b denote areas of major differences).

Above average conformational differences between the three structures are localized to four regions: residues 22−29, residues 100−112, residues 147−170, and residues 226−238. The first section (residues 22−29) corresponds to a loop (denoted a in Figure 1) between $\beta$-strands 1 ($\beta$1) and 2 ($\beta$2) in the N-terminal domain of APH(3′)-IIIa. This loop forms part of the APH(3′)-IIIa nucleotide-binding site and is analogous to the P-loop of eukaryotic protein kinases. The significant shift observed in this region reflects a real difference between the apoenzyme structure and the ADP and AMPPNP complexes. In the apoenzyme, the polypeptide shifts downward into the nucleotide-binding pocket relative to its position in the complexes and occupies some of the cavity resulting from the lack of bound nucleotide.

As described above in reference to the ADP and AMPPNP complexes, residues 100−112 and residues 226−238 form parts of loop regions in the APH(3′)-IIIa molecule, and the quality of the density in this region is poor in all three structures. Thus, differences between the structures are likely the result of the inherent flexibility of the protein in these areas and not differences attributable to nucleotide binding.

With respect to residues 147−170, the proposed antibiotic binding site, this segment of the enzyme has a dramatically different conformation in the absence of bound nucleotide compared to APH(3′)-IIIa in the nucleotide-bound state

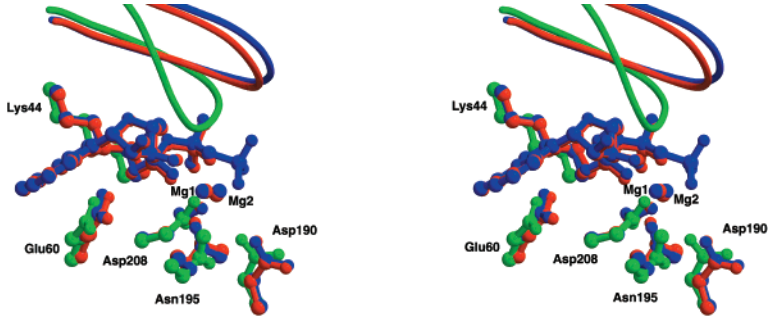


FIGURE 2: Stereo ball-and-stick drawing of the nucleotide-binding pockets of APH(3′)-IIIa. The structures of the apoenzyme, ADP, and AMPPNP complexes are drawn in green, red, and blue, respectively. In addition to the nucleotide molecule, the figure also depicts the conserved amino acid residues of the binding pocket and the two metal ions in ball-and-stick form. The flexible loop positioned over the binding pocket is also shown.

(denoted as b in Figure 1). However, this different conformation is also unlikely linked to the absence or presence of a nucleotide but is a direct result of differing crystal contacts between the apoenzyme and the nucleotide complexes in this region, as well as a consequence of the presence of the intermolecular disulfide bond. As mentioned above, in the ADP and AMPPNP crystals the intermolecular disulfide bond links the two molecules in the asymmetric unit, while in the apoenzyme crystal, the link is between adjacent asymmetric units (in this crystal form there is only a single molecule per the asymmetric unit).

*Nucleotide Binding Site.* The active site of APH(3′)-IIIa is located in a cleft formed between the N- and C-terminal lobes of the enzyme. Residues from both lobes contribute to the formation of the large, relatively hydrophobic cavity in which the nucleotide binds. As can be seen in Figure 2, the conformations of the nucleotides and conserved active site are essentially identical in the ADP and AMPPNP complexes, and interactions between the nucleotides and the protein are very similar. These interactions are summarized schematically in Figure 3.

The adenine ring is buried, forming van der Waals interactions with Tyr42, Glu92, and Phe197. The interaction with Tyr42 is a stacking of the base with the aromatic ring of the tyrosine side chain. The adenine ring also forms two hydrogen-bonding interactions with the polypeptide backbone that forms the structural scaffold of the binding pocket. These consist of an interaction between the N1 atom of the nucleotide and the backbone amide of Ala93 and one between the N6 atom and the backbone carbonyl oxygen of Ser91. The ribose component interacts with the protein via a single hydrogen bond between the O3′ oxygen of the sugar and the carbonyl oxygen of Ser194.

The interactions of the nucleotide phosphate groups involve the side chains of conserved active site residues and metal ions. The α-phosphate group interacts with two water molecules, as well as with the protein via a hydrogen bond with the NZ atom of Lys44. This residue is positioned over the top of the binding pocket and is conserved both in all APH enzymes and in ePK's (*3*). In both nucleotide complexes, the $\beta$-phosphate group forms one hydrogen bond with a water molecule and two hydrogen bond interactions with protein atoms: one between the O1B atom and the Lys44 NZ atom and a second between the O2B oxygen atom and the OG atom of Ser27. The latter residue is conserved in most APH(3′) enzymes but not in ePK's. In addition to its

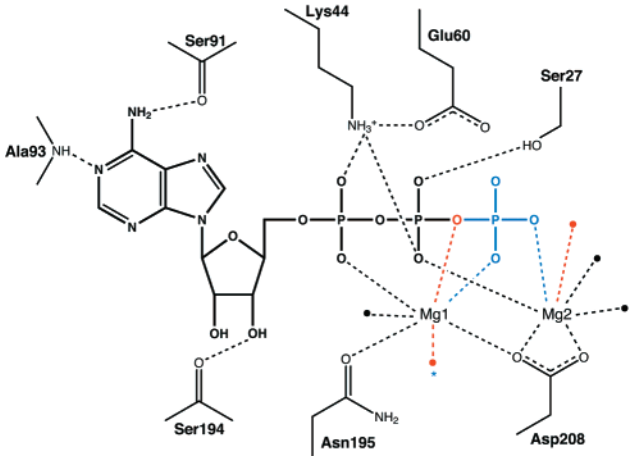


FIGURE 3: Schematic representation of the hydrogen bond interactions between APH(3′)-IIIa and ADP or ATP based on the crystal structures of the APH(3′)-IIIa·ADP and APH(3′)-IIIa·AMPPNP complexes. Interactions common to the nucleotides and the enzyme are shown in black, while those unique to ADP are shown in red and those unique to ATP are shown in light blue. The asterisk denotes a water molecule that is not observed in the AMPPNP complex. Note that the ATP depicted in the figure has an oxygen atom bridging the $\beta$- and $\gamma$-phosphate atoms, while the ATP analogue AMPPNP in the APH(3′)-IIIa·AMPPNP complex has an NH group.

interactions with the protein, the $\beta$-phosphoryl group of ADP also coordinates with the magnesium ions associated with the enzyme (see Figure 3).

The $\gamma$-phosphate present in the AMPPNP structure displaces two water molecules present in the ADP complex. There are no direct interactions between the $\gamma$-phosphate of the AMPPNP molecule and the protein. In addition to interactions with two water molecules, the terminal phosphate coordinates to the magnesium ions in the active site. Following the nomenclature adopted with the structures of cAPK and the $\gamma$ subunit of glycogen phosphorylase kinase (Phk$\gamma$), the two metal ions in the active site of these enzymes are commonly referred to as Mg1 and Mg2. The O1G and O3G atoms of AMPPNP coordinate to Mg1 and Mg2, respectively. Although the presence of the additional phosphate group also appears to lead to different conformations for the side chains of Glu24 and Met26 in the structure of the AMPPNP complex, a more likely alternative explanation exists. In the structure of the AMPPNP complex, this region of the polypeptide chain exhibits elevated thermal factors and poorly defined electron density. The fact that these side

chains are positioned differently in the two molecules in the APH(3′)-IIIa·AMPPNP asymmetric unit lends further credence to the idea that these differences are likely the result of differential fitting of the side chains to poor density. The resolution of the AMPPNP data set was not sufficient to enable the identification or refinement of discrete alternative conformations of these residues. It does appear, however, that the presence of AMPPNP in the nucleotide-binding pocket instead of ADP leads to an increase in the flexibility of this segment of the polypeptide chain.

Superposition of the ADP and AMPPNP complexes indicates that the positions of the active site magnesium ions remain essentially unchanged between the two complexes (see Figure 2). There are, however, differences in the identity of the coordinating species. Both magnesium ions in the ADP complex are coordinated in an octahedral fashion, with Mg1 coordinated by two oxygen atoms from the α- and β-phosphate groups of the ADP molecule, the amide oxygen of Asn195, a carboxyl oxygen from Asp208, and two water molecules. The second magnesium ion, Mg2, is coordinated by an oxygen atom from the β-phosphate of ADP, two carbonyl oxygens from Asp208, and three water molecules. The geometry of the metal ligands in the AMPPNP complex is also octahedral and is similar to that observed in the ADP complex. Coordination of Mg1 in this structure is via two oxygen atoms from the α- and γ-phosphates of AMPPNP, an amide oxygen from Asn195, a carboxyl oxygen from Asp208, and a water molecule. Although not convincing enough to warrant inclusion in the model, there is some evidence for a second coordinated water molecule (noted with an asterisk in Figure 3). In the AMPPNP complex, Mg2 is coordinated by two carboxyl oxygens from Asp208, two oxygens from the β- and γ-phosphate groups of AMPPNP, and two water molecules.

## DISCUSSION

We have determined the structures of APH(3′)-IIIa in complex with the nonhydrolyzable ATP analogue AMPPNP and in its apoenzyme form without bound nucleotide. In addition, we have further refined the ADP complex published previously. These structure determinations were undertaken in an effort to further our understanding of the mechanism by which this enzyme carries out the inactivation of aminoglycoside antibiotics. Discussion of the results of these structural studies falls naturally into two parts. The first of these concerns the differences between the apoenzyme and the structures with bound nucleotide. What are the structural consequences of nucleotide binding to APH(3′)-IIIa and how do these compare to those observed in the structurally related eukaryotic protein kinases? The second area of discussion concerns the structures of APH(3′)-IIIa in complex with ADP and AMPPNP. Can these structures provide insight into the mechanism of phosphoryl transfer by this enzyme?

*Structural Consequences of Nucleotide Binding.* The most notable feature that strikes an observer comparing the structures of the APH(3′)-IIIa apoenzyme with the two structures with bound nucleotide is that they are remarkably similar. The majority of the positional differences between the structures are confined to surface loop regions in which flexibility is not unexpected. There is one region in which positional variability appears to be relevant to enzyme function. The only change in the polypeptide backbone position directly attributable to the absence of nucleotide in the apoenzyme structure is a shift in the polypeptide backbone to occupy the space that would be occupied by the nucleotide (rmsd of 1.7 Å for main chain atoms of residues 20−33). In contrast, the conformation of the polypeptide backbone of the APH(3′)-IIIa·nucleotide complexes is very similar in this area (rmsd of 0.4 Å for main chain atoms of residues 20−33). This region covers the phosphate-binding subsite of the nucleotide-binding site and is analogous to the G-X-G-X-X-G nucleotide-positioning motif found in the catalytic core of eukaryotic protein kinases such as cAPK (*28*). The characteristically flexible glycine-rich motif, which forms a shield over the phosphate groups of the bound nucleotide, is also found in other nucleotide-binding proteins, including nucleotidyltransferases and ATPases (*29*). The flexibility of this region of the active site in the APH(3′)-IIIa structures may facilitate the binding and release of nucleotides that occurs over the course of the catalytic cycle. Recent kinetic evidence from site-directed mutants suggests that the loop may also play a stabilizing role during phosphoryl transfer (P. Thompson, and G. Wright, personal communication).

Although both the G-X-G-X-X-G motif in ePK's and the corresponding loop structure in APH(3′)-IIIa serve to shield the nucleotide-binding pockets, the conformations of the two are distinctly different. As a consequence of a one-residue insertion, the loop is larger in APH(3′)-IIIa and forms a looser turn than is observed in the ePK structures (*12*). In the APH(3′)-IIIa complexes, the nucleotide interacts with this loop via a single hydrogen bond to the Ser27 OG atom. This is in contrast to ePK's such as cAPK and cyclin-dependent protein kinase in which interactions with the bound nucleotide are via hydrogen bonds to the backbone amide groups of the G-X-G-X-X-G motif (*31*, *32*). Note that although this motif is observed in a number of ePK's, the protein−nucleotide interactions in the various ePK's are not the same. In Phkγ, interaction between the loop and nucleotide does not involve main chain amides at all but instead occurs through a serine OG atom as observed in APH(3′)-IIIa (*33*). This is despite a three-dimensional loop structure that more closely resembles that of other ePK's. The variability in hydrogen bonding observed in the enzymes suggests that this loop may simply serve as a shield for the nucleotide-binding site and that the G-X-G-X-X-G sequence motif of ePK's, while reflecting a conserved structural feature, does not reflect the conservation of specific protein−nucleotide interactions.

That the structural differences between the APH(3′)-IIIa apoenzyme and the nucleotide-bound complexes are relatively minor and confined to the area surrounding the active site is in marked contrast to the significant domain shifts observed in some ePK's upon nucleotide binding (*34*). Protein footprinting studies have shown that the binding of ATP causes conformational changes in the active site of cAPK which are consistent with a change from an open active site conformation to a closed form that is essential for phosphoryl transfer (*35*). This conformational change can be substantial. In the transition between the open and closed conformations of cAPK, the C-terminal lobe rotates by over 10° with respect to a rotation axis relating the two lobes of the molecule (*36*). Such substrate-induced conformational

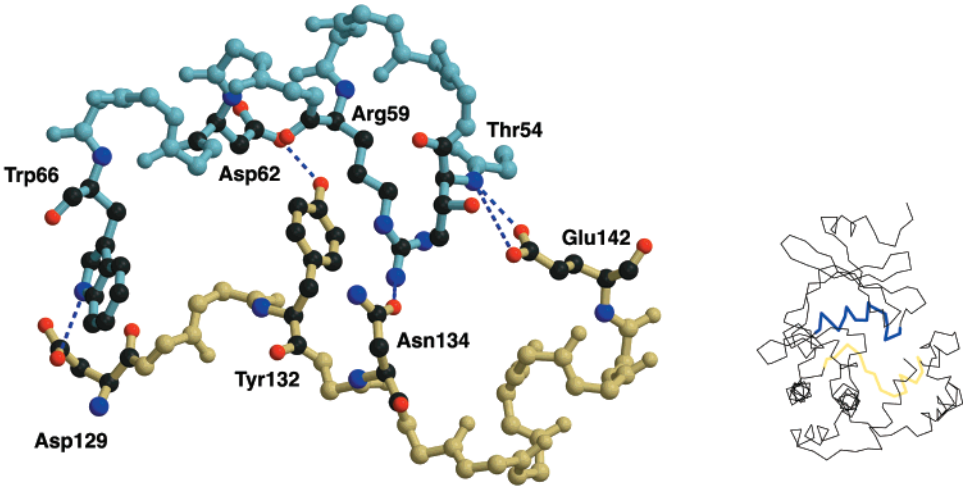


FIGURE 4: Ball-and-stick drawing (at left) showing hydrogen bond interactions (dashed blue lines) in the hinge region of the APH(3′)-IIIa molecule. Residues from the N- and C-terminal lobes are depicted in blue and tan, respectively. For clarity, side chain atoms are only drawn for residues that are involved in hydrogen bonds. The α carbon trace (at right) shows the region of the APH(3′)-IIIa molecule highlighted in the ball-and-stick portion of the figure.

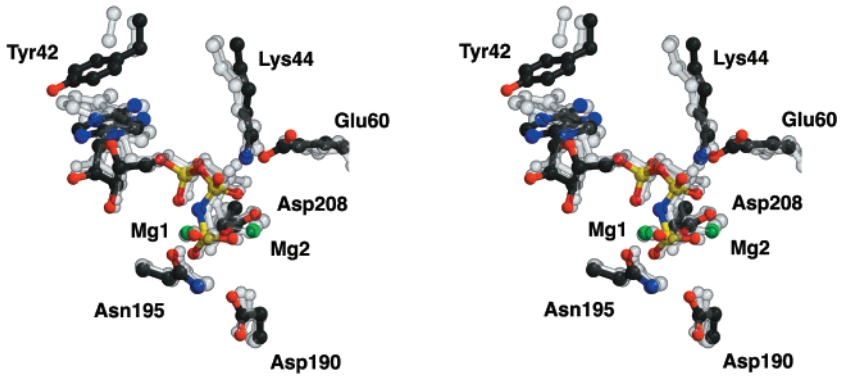


FIGURE 5: Stereo ball-and-stick drawing showing the superimposed structures of the AMPPNP complex of APH(3′)-IIIa (color) and those of the eukaryotic protein kinases cAPK and Phk$\gamma$ (transparent gray). The figure shows the nucleotide, metal ions, and the conserved active site side chains Lys44, Glu60, Asp190, Asn195, and Asp208. Also shown are Tyr42, which participates in a stacking interaction with the nucleotide in the APH(3′)-IIIa structures, and the equivalent alanine residues in cAPK and Phk$\gamma$.

changes have also been observed in cyclin-dependent protein kinases (*37*).

What is the origin of the rigidity of the APH(3′)-IIIa molecule, as compared to the eukaryotic protein kinases? In both cases, the two lobes of the protein are associated mainly via two mechanisms: a covalent linkage between the two lobes and noncovalent interactions. The covalent link in APH(3′)-IIIa is a short segment of $\beta$-structure and α-helix comprising residues 93−106 in APH(3′)-IIIa. An analogous linker is found in a similar position in the structure of the catalytic cores of ePK's. The region of noncovalent interactions between domains, the so-called "domain linker" or "domain hinge" is located on the opposite side of the molecule from the nucleotide-binding pocket and in APH(3′)-IIIa includes interactions between residues of helix α2 from the N-terminal lobe and residues between helices α4 and αA of the C-terminal lobe (Figure 4). As mentioned previously, distinct "open" and "closed" conformations have been observed in the structures of eukaryotic protein kinases. The hinge region of the protein kinase structure has been proposed to act as the pivot point about which the two domains move.

One possible explanation for the lack of nucleotide-induced domain movement in APH(3′)-IIIa may be the increased number of interactions between the domains in the linker and hinge regions. While the helix in cAPK that is analogous to α2 in APH(3′)-IIIa is in a similar position, the loop in the C-lobe is noticeably different. This is in part due to the fact that the adjacent large antibiotic-binding loop (residues 147−170) must be accommodated in the APH(3′)-IIIa structure, but is not found in the kinase structures. As a result of the different orientations of these segments, the number of hydrogen bond interactions in the hinge is lower in kinases such as cAPK (two) than in APH(3′)-IIIa (five; see Figure 4). The more extensive hydrogen bond and van der Waals interactions present in the structure would make interdomain movement in APH(3′)-IIIa energetically unfavorable. Similar interactions are observed in both crystal forms examined, suggesting that this is a characteristic of the protein, not simply a consequence of a particular crystal packing arrangement.

Protein kinases are involved in the important areas of cellular regulation and signal transduction. This critical function requires that there be a mechanism by which the activity of these enzymes can be tightly controlled. Perhaps the interdomain flexibility present in the protein kinase confers additional specificity. In contrast to the protein kinases, the requirement for tight regulation of aminoglycoside-modifying enzymes such as APH(3′)-IIIa does not appear to be critical. In fact, it appears to be to the organism's

advantage to have an enzyme present in the cell in its active conformation, ready to bind and inactivate aminoglycoside molecules. This ability may in fact be of the utmost importance to the cell, since the uptake of small amounts of aminoglycoside into the cell may be a key first step in the bactericidal effect of these antibiotics. A model for aminoglycoside action has been proposed in which the initial entry of small amounts of aminoglycoside leads to the formation of misfolded proteins, loss of membrane integrity, the influx of additional aminoglycoside, and the saturation of all ribosomes (*38*). Given such a mechanism, it is clear that regulation of aminoglycoside phosphotransferase via lobe movements such as that seen in protein kinases is not advantageous and has either not arisen in APH(3′)-IIIa or has been dispensed with through the process of natural selection.

*Insight into Mechanism of Phosphate Transfer*. While the differences in backbone conformation between the apoenzyme and nucleotide-bound structures of APH(3′)-IIIa were minor compared to those observed in eukaryotic protein kinases, the differences are large compared to those between the ADP and AMPPNP complexes of APH(3′)-IIIa. The two regions of above average positional deviation between backbone atoms of the ADP and AMPPNP complexes are the P-loop (residues 23−25) and domain linker (residues 102−104). However, the magnitude of the deviation is much smaller in this case (<1.6 Å as compared to >5 Å for the apoenzyme comparison).

In addition to the small changes in backbone position, there are subtle differences between the two nucleotide complexes in the active site (see Figure 4). Following superposition of the structures of the ADP and AMPPNP complexes, the nucleotides and the conserved features of the active site are very similar. The only noticeable difference between the complexes is the presence of the additional phosphate group in AMPPNP and a change in the coordination of the active site metal ions. There are five active site residues that are absolutely conserved among both APH enzymes and eukaryotic protein kinases: Lys44, Glu60, Asp190, Asn195, and Asp208. In APH, these residues, along with the two metal ions, form a network of interactions that fix the nontransferable phosphate groups of the nucleotide. The position of these conserved residues is essentially identical in the two APH(3′)-IIIa complexes. Although the position of the two magnesium ions remains the same in the two structures, their coordination has changed to accommodate the additional atoms of the AMPPNP molecule. The two active site magnesium ions of APH(3′)-IIIa facilitate the binding of nucleotides to enzyme, both in the ADP and in the AMPPNP bound forms. The enzyme is able to cycle between the two forms without the necessity for rearrangement of or significant changes in the coordination of the metal ions.

The structures of the catalytic subunit of cAMP-dependent protein kinase (cAPK) with ATP, Mn, and peptide inhibitor (PDB entry 1ATP), Phk$\gamma$ in complex with ATP (PDB entry 1PHK), and that of APH(3′)-IIIa·AMPPNP were superimposed using the coordinates of the conserved active site residues (Lys44, Glu60, Asp190, Asn195, and Asp208 and their ePK equivalents). The active site residues conserved in both APH's and ePK's superimpose closely, as do the two active site metal ions. Furthermore, the $\gamma$-phosphate of AMPPNP in the APH complex occupies the same location as that of the $\gamma$-phosphate in both ePK structures. Despite the high degree of structural similarity, there are noticeable differences as well. The superposition of the nucleotides becomes poorer as one moves from the $\gamma$-phosphate toward the adenine component of the nucleotide, and the adenine ring of the ePK's is rotated by approximately 40° with respect to that observed in the APH complexes. In the APH enzyme, the adenine ring participates in a stacking interaction with the aromatic side chain of Tyr42. This residue is highly conserved in APH(3′) enzymes, being either a phenylalanine or tyrosine residue. The corresponding residue in the structures of the protein kinases is alanine, precluding a stacking interaction and necessitating the alternate packing arrangement for the adenine ring observed in these structures. Although different in the two classes of enzymes, the significance of this observation is not clear, given the high degree of similarity observed in the rest of the active site. However, this difference in nucleotide binding between the two classes of enzymes opens up the possibility of exploiting the differences via structure-based drug design to develop possible therapeutic agents for the treatment of aminoglycoside resistance.

The similarity between the active sites of APH(3′)-IIIa and the two eukaryotic protein kinases is striking, both in terms of the orientation of conserved residues and in terms of bound nucleotide and metal ions. This is compelling evidence for a common mechanism of phosphoryl transfer among these disparate groups of enzymes. A definitive explanation of the precise mechanism by which protein kinases catalyze the transfer of phosphoryl groups remains elusive, with experimental evidence to support both an associative ($S_N2$-like) (*39*) and dissociative ($S_N1$-like) (*40*) transition state. Our structural studies suggest that information gleaned about the mechanism of phosphoryl transfer in APH(3′)-IIIa will also be applicable to that of eukaryotic protein kinases.

## ACKNOWLEDGMENT

We thank the past and present members of the Berghuis laboratory for their assistance and suggestions.

## REFERENCES

1. Davies, J. (1996) *Nature 383*, 219−220.
2. Davies, J. (1994) *Science 264*, 375−382.
3. Wright, G. D., Berghuis, A. M., and Mobashery, S. (1998) *Adv. Exp. Med. Biol. 456*, 27−69.
4. Neu, H. C. (1992) *Science 257*, 1064−1072.
5. Carter, A. P., Clemons, W. M., Brodersen, D. E., Morgan-Warren, R. J., Wimberly, B. T., and Ramakrishnan, V. (2000) *Nature 407*, 340−348.
6. Begg, E. J., and Barclay, M. L. (1995) *Br. J. Clin. Pharmacol. 39*, 597−603.
7. Shaw, K. J., Rather, P. N., Hare, R. S., and Miller, G. H. (1993) *Microbiol. Rev. 57*, 138−163.
8. McKay, G. A., Thompson, P. R., and Wright, G. D. (1994) *Biochemistry 33*, 6936−6944.
9. Thompson, P. R., Hughes, D. W., and Wright, G. D. (1996) *Biochemistry 35*, 8686−8695.
10. McKay, G. A., and Wright, G. D. (1995) *J. Biol. Chem. 270*, 24686−24692.
11. Boehr, D. D., Thompson, P. R., and Wright, G. D. (2001) *J. Biol. Chem.* (in press).
12. Hon, W. C., McKay, G. A., Thompson, P. R., Sweet, R. M., Yang, D. S., Wright, G. D., and Berghuis, A. M. (1997) *Cell 89*, 887−895.

13. Thompson, P. R., Hughes, D. W., and Wright, G. D. (1996) *Chem. Biol. 3*, 747−755.
14. Daigle, D. M., McKay, G. A., Thompson, P. R., and Wright, G. D. (1999) *Chem. Biol. 6*, 11−18.
15. Daigle, D. M., McKay, G. A., and Wright, G. D. (1997) *J. Biol. Chem. 272*, 24755−24758.
16. Otwinowski, Z., and Minor, W. (1997) *Methods Enzymol. 276*, 307−326.
17. Brünger, A. T., Adams, P. D., Clore, G. M., DeLano, W. L., Gros, P., Grosse-Kunstleve, R. W., Jiang, J.-S., Kuszewski, J., Nilges, M., Pannu, N. S., Read, R. J., Rice, L. M., Simonson, T., and Warren, G. L. (1998) *Acta Crystallogr. D54*, 905−921.
18. Read, R. J. (1986) *Acta Crystallogr. A42*, 140−149.
19. Kleywegt, G. J., and Brünger, A. T. (1996) *Structure 4*, 897−904.
20. Brünger, A. T. (1992) *Nature 355*, 472−474.
21. Brünger, A. T., and Nilges, M. (1993) *Q. Rev. Biophys. 26*, 49−125.
22. Brünger, A. T. (1993) *Acta Crystallogr. D49*, 24−36.
23. Brünger, A. T. (1997) *Methods Enzymol. 277*, 366−396.
24. Brünger, A. T. (1993) *X-PLOR, version 3.1: a system for X-ray crystallography and NMR*, Yale University Press, New Haven, CT.
25. Laskowski, R. A., MacArthur, M. W., Moss, D. S., and Thornton, J. M. (1993) *J. Appl. Crystallogr. 26*, 283−291.
26. Morris, A. L., MacArthur, M. W., Hutchinson, E. G., and Thornton, J. M. (1992) *Proteins 12*, 345−364.
27. Kleywegt, G. J. (1996) *Acta Crystallogr. D52*, 842−857.
28. Hanks, S. K., and Hunter, T. (1995) *FASEB J. 9*, 576−596.
29. Smith, C. A., and Rayment, I. (1996) *Biophys. J. 70*, 1590−1602.
30. Zheng, J. H., Trafny, E. A., Knighton, D. R., Xuong, N. H., Taylor, S. S., TenEyck, L. F., and Sowadski, J. M. (1993) *Biochemistry 32*, 2154−2161.
31. Schulze-Gahmen, U., DeBondt, H. L., and Kim, S. H. (1996) *J. Med. Chem. 39*, 4540−4546.
32. Owen, D. J., Noble, M. E., Garman, E. F., Papageorgiou, A. C., and Johnson, L. N. (1995) *Structure 3*, 467−482.
33. Zheng, J., Knighton, D. R., Xuong, N. H., Taylor, S. S., Sowadski, J. M., and Ten Eyck, L. F. (1993) *Protein Sci. 2*, 1559−1573.
34. Cheng, X., Shaltiel, S., and Taylor, S. S. (1998) *Biochemistry 37*, 14005−14013.
35. Narayana, N., Cox, S., Nguyen-huu, X., Ten Eyck, L. F., and Taylor, S. S. (1997) *Structure 5*, 921−935.
36. Heitz, F., Morris, M. C., Fesquet, D., Cavadore, J. C., Doree, M., and Divita, G. (1997) *Biochemistry 36*, 4995−5003.
37. Davis, B. D. (1987) *Microbiol. Rev. 51*, 341−350.
38. Hutter, M. C., and Helms, V. (1999) *Protein Sci.* 8, 2728−2733.
39. Kim, K., Parang, K., Laue, O. D., and Cole, P. A. (2000) *Bioorg. Med. Chem. 8*, 1263−1268.

BI010504P